The essence of Biot waves in an oscillator with two degrees of freedom

Dominik Kern[a,★] [iD] , Thomas Nagel[a] [iD]

[a] Technische Universität Bergakademie Freiberg, Freiberg, Germany

★ corresponding author: dominik.kern.ifgt@gmail.com

Abstract: *In poroelastic media, i.e., porous structures whose pores contain fluid, a kind of waves can be observed that does not occur in elastic media, the so-called slow P-waves or Biot waves, which may be perceived as opaque when first encountered. In this paper, we pursue two goals: firstly, we want to provide a simple explanatory model of these waves and, secondly, we want to prepare the reader for Biot's seminal paper. We discretize a finite poroelastic waveguide by Galerkin's method to arrive at a mechanical system with 2 degrees of freedom and solve the eigenvalue problem of free oscillations. This oscillator representation (ODE) is simpler than the wave representation (PDE) while maintaining salient features of poroelastodynamics and offering a different perspective. In fact, an oscillation is a standing wave with wave velocity and wave length being related to frequency and domain length. In this reduced model, slow P-waves, when they exist, correspond to an oscillation with large phase shift and fast P-waves to an oscillation with small phase shift.*

The intended audience are engineering or physics graduate students with basic knowledge of linear oscillations, linear differential equations and some understanding of biphasic media.

Keywords: wave propagation, porous media, poroelasticity, linear differential equations, Biot waves, slow P-waves

1 Introduction

Poroelasticity is commonly used to model quasistatic deformations of soils, rocks or biological tissues, in addition to the solid matrix it considers the pore fluid, too. The evaluation of seismic signals in geology or ultrasound waves in medical technology often assumes elasticity as the underlying theoretical framework, neglecting the influence of the pore fluid. In elastic media, there are two types of waves: pressure-waves (P-waves) and shear-waves (S-waves), which are also named primary and secondary waves, respectively, because the former are faster than the latter. A qualitative difference between poroelasticity and elasticity when it comes to dynamic problems in fully saturated media is the occurrence of a new type of wave, a slow P-wave [1, 2] in addition to the fast P-waves, which corresponds to the P-waves in elastic media. There are even more of these slow P-waves in porous media whose pore space is filled with distinct fluid phases, i.e., under conditions of partial saturation [3, 13]. Often, these kinds of waves are ignored, since they are highly dissipative, but also because they seem, to a certain degree, to be somewhat mysterious, even to some geophysicists. This may be rooted in the fact that they are not easily observed and were experimentally demonstrated much later than theory predicted their existence [12]. We wish to aid students and researchers starting to work on biphasic dynam-

ics in their "de-mystification" and try to illustrate Biot waves as simply as possible by reducing the wave propagation problem in a continuous domain, given by partial differential equations (PDEs), to free oscillations of a discrete system, given by ordinary differential equations (ODEs). Such a reduced model is often more easily accessible to graduates with a typical background from an engineering mechanics syllabus centered around mass-spring-damper systems. Even though this description is simpler than in the original papers by Biot [1, 2], it retains shared features key to their phenomenology, such as mass coupling and some characteristic parameter ratios. Familiarity with non-dimensionalization [9, 10] would be a key asset for understanding the paper, since we directly start from well-established models in their non-dimensional formulation. We also assume familiarity with static biphasic theory and refer to textbooks [4, 14, 15] for further details.

We review S-waves in section 2, where only one kind of wave exists in contrast to P-waves. With the aid of this simpler case we introduce the path to discretization and we also notice differences in wave propagation between poroelastic and elastic media. Next, we move on to the main subject of the paper, the model for P-waves in section 3, with which we perform a modal analysis in section 4, and discuss the results in section 5.

We use the same characteristic frequency

$$f_{\mathrm{c}} = \frac{1}{2\pi} \frac{\mu n}{\kappa \varrho_{\mathrm{f}}}, \tag{1}$$

as Biot does, to define *low* ($f < f_{\mathrm{c}}$) and *high* ($f > f_{\mathrm{c}}$) frequencies. This characteristic frequency depends on material parameters only and is used as reference for both, S- and P-waves.

2 S-waves as Preliminary

We reduce propagation of shear waves in an one-dimensional poroelastic bar to oscillations of a two-body system, with which we perform a modal analysis.

2.1 Continuum model

Our point of departure is the set of mass and momentum balance, see equations (5.8) and (5.15) in Verruijt's textbook [14], in non-dimensional formulation for one-dimensional shear waveguides

$$\frac{n}{\rho}\ddot{u}_{\mathrm{f}} + \frac{n\tau}{\rho}(\ddot{u}_{\mathrm{f}} - \ddot{u}_{\mathrm{s}}) + nD_S(\dot{u}_{\mathrm{f}} - \dot{u}_{\mathrm{s}}) = 0, \tag{2a}$$

$$(1-n)\ddot{u}_{\mathrm{s}} - \frac{n\tau}{\rho}(\ddot{u}_{\mathrm{f}} - \ddot{u}_{\mathrm{s}}) - nD_S(\dot{u}_{\mathrm{f}} - \dot{u}_{\mathrm{s}}) - u_{\mathrm{s}}'' = 0, \tag{2b}$$
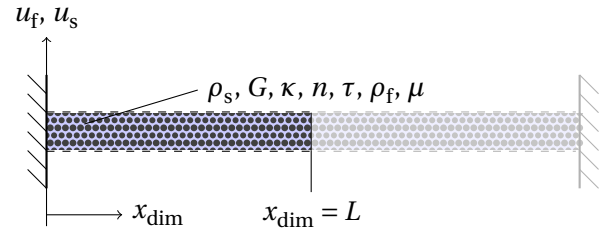
Figure 1 – Continuous model for S-waves: one-dimensional, poroelastic bar with fixed, undrained left end ($x_{\mathrm{dim}} = 0$) and symmetry boundary condition at the right end ($x_{\mathrm{dim}} = L$).
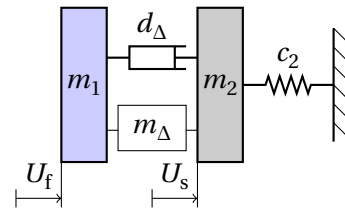
Figure 2 – Multibody-system representing a reduced model for S-waves in a poroelastic bar.

with total displacement of the fluid phase u_{f} and total displacement of the solid phase u_{s}, and where $\dot{\square}$ denotes partial derivative with respect to time t and $\square'$ with respect to spatial coordinate x.

For non-dimensionalization we refer positions to bar length L and time to $T = L\sqrt{m_{\mathrm{v}}\varrho_{\mathrm{s}}}$. The *ab initio* non-dimensional parameters are: porosity n and tortuosity factor τ. The latter appears as an added-mass (inertial) effect due to fluid acceleration along curved flow paths. The non-dimensional parameters

$$\rho = \frac{\varrho_{\mathrm{s}}}{\varrho_{\mathrm{f}}}, \tag{3}$$

$$D_S = \frac{n\mu L}{\kappa\sqrt{G\varrho_{\mathrm{s}}}}, \tag{4}$$

are related with the original parameters: ϱ_{f} fluid density, ϱ_{s} solid density, G shear modulus (bulk, drained), μ viscosity of the fluid, and κ intrinsic permeability. By *fluid* and *solid* we refer to the pure material (massive) and by *bulk* to the porous matrix (averaged properties of cell/truss structure). As an example, we consider the bar shown in figure 1 with the numerical values listed in appendix A. This bar of length L (dimensional model) corresponds to one half of a bar of length $2L$ fixed on both ends. The mechanical boundary conditions are that of a fixed, undrained left end and a symmetry boundary

condition at the right end

$$u_\text{f}(t,0) = 0, \tag{5a}$$

$$u_\text{s}(t,0) = 0, \tag{5b}$$

$$u_\text{f}'(t,1) = 0, \tag{5c}$$

$$u_\text{s}'(t,1) = 0. \tag{5d}$$

If we were interested in asymmetric mode shapes of the original bar, then we had to take its full length into account. However, the symmetric mode shapes are sufficient for our purpose and that way we keep this example aligned with the upcoming model for P-waves. For sake of completeness, we note that the field equation (2) inherently contains the assumption of plane waves (infinite cross-sectional area) that we may imagine as a periodic boundary condition on top and bottom (flow top-out equals bottom-in and vice versa) conserving the fluid mass.

2.2 Model reduction

We use separation of variables and assume a solution of the form given by a product of a function in space and a function in time. As function in space we choose the base mode shape (first eigenmode) of an elastic bar complying with the boundary conditions (5)

$$u_\text{f}(t,x) = U_\text{f}(t) \sin\left(\pi\left(\frac{1}{2} + k\right)x\right), \tag{6a}$$

$$u_\text{s}(t,x) = U_\text{s}(t) \sin\left(\pi\left(\frac{1}{2} + k\right)x\right), \tag{6b}$$

with mode number $k \in \mathbb{N}$. For a finer approximation, one may use more ansatz functions, however we are going for the simplest model possible. According to Galerkin's method [5], we plug ansatz (6) into PDE (2), weight the residuum and integrate over the domain. This discretization eliminates the dependency on the spatial coordinate x, here shown for equation (2a) and base mode ($k = 0$)

$$\int_0^1 \left(\frac{n(1+\tau)}{\rho}\ddot{U}_\text{f}(t) - \frac{n\tau}{\rho}\ddot{U}_\text{s}(t) \right.$$
$$\left. + nD_S\left(\dot{U}_\text{f}(t) - \dot{U}_\text{s}(t)\right)\right)\sin^2\left(\frac{\pi}{2}x\right)\mathrm{d}x = 0, \tag{7}$$

noting that we used the same functions for the spatial parts of the ansatz and weights (Bubnov-Galerkin method). For sake of completeness, these functions are also referred to as trial and test functions, respectively.

Hence, we are left with a system of two coupled ODEs, which corresponds to the multibody-system shown in figure 2. Sorting for displacement, velocity and acceleration of fluid and solid gives the meaning of the multibody-system parameters as springs, dashpots and masses

$$m_1 = I_{11}\frac{n}{\rho}, \tag{8a}$$

$$m_2 = I_{22}(1 - n), \tag{8b}$$

$$m_\Delta = I_{12}\frac{n\tau}{\rho}, \tag{8c}$$

$$d_\Delta = I_{12}nD_\text{S}, \tag{8d}$$

$$c_2 = I_{22}\left(\frac{\pi}{2}\right)^2, \tag{8e}$$

with the integrals over the products of ansatz and weight functions

$$I_{11} = I_{12} = I_{22} = \int_0^1 \sin^2\left(\frac{\pi}{2}x\right)\mathrm{d}x = \frac{1}{2}. \tag{9}$$

Although, here the I_{ij} share the same value, we keep separate variables to point out, where different ansatz functions for fluid and solid motion would enter. All parameters given by equation (8) are common for multibody-systems, except the mass coupling m_Δ, which results from the tortuosity. In the customary notation of multibody dynamics, we have an equation of motion

$$\mathbf{M}\ddot{\mathbf{q}} + \mathbf{D}\dot{\mathbf{q}} + \mathbf{C}\mathbf{q} = \mathbf{0}, \tag{10}$$

with position vector

$$\mathbf{q} = \left[\begin{array}{c} U_\text{f}(t) \\ U_\text{s}(t) \end{array}\right], \tag{11}$$

mass matrix

$$\mathbf{M} = \left[\begin{array}{cc} m_1 + m_\Delta & -m_\Delta \\ \text{sym.} & m_2 + m_\Delta \end{array}\right], \tag{12}$$

damping matrix

$$\mathbf{D} = \left[\begin{array}{cc} d_\Delta & -d_\Delta \\ \text{sym.} & d_\Delta \end{array}\right], \tag{13}$$

and stiffness matrix

$$\mathbf{C} = \left[\begin{array}{cc} 0 & 0 \\ \text{sym.} & c_2 \end{array}\right]. \tag{14}$$

Evaluation of the *swap relation* [6]

$$\mathbf{M}^{-1}\mathbf{D}\mathbf{M}^{-1}\mathbf{C} \neq \mathbf{M}^{-1}\mathbf{C}\mathbf{M}^{-1}\mathbf{D} \tag{15}$$

reveals that the damping is non-modal due to frictional fluid flow in the pores; assuming an inviscid fluid ($\mu = 0$) it becomes modal (or rather undamped). If, additionally, tortuosity vanishes ($\mu = 0$ and $\tau = 0$), then the masses m_1 and m_2 were decoupled. Mathematically speaking, diagonalization with the eigenvectors of the undamped system is impossible. Consequently, we expect complex eigenvectors, which is nothing out of the ordinary and simply introduces phase-shifts other than integer multiples of π.

2.3 Modal analysis

The first choice for linear systems of ODEs like (10) is an exponential ansatz

$$\mathbf{q}(t) = \hat{\mathbf{q}}e^{\delta t} \quad \text{with} \quad \mathbf{q}(t) = \begin{bmatrix} U_{\mathrm{f}}(t) \\ U_{\mathrm{s}}(t) \end{bmatrix}, \qquad (16)$$

whose real part has the physically meaningful interpretation of a position

$$\Re\left\{\hat{U}_{\mathrm{f}}e^{\delta t}\right\} = |\hat{U}_{\mathrm{f}}|e^{-t/T}\cos(\omega t + \varphi_{\mathrm{f}}), \qquad (17a)$$

$$\Re\left\{\hat{U}_{\mathrm{s}}e^{\delta t}\right\} = |\hat{U}_{\mathrm{s}}|e^{-t/T}\cos(\omega t + \varphi_{\mathrm{s}}), \qquad (17b)$$

while its imaginary part is ignored. The real part of the coefficient $\Re\{\delta\} = -\frac{1}{T}$ describes the decay and the imaginary part $\Im\{\delta\} = \omega$ periodic oscillations (same coefficient for both components of the position vector $\mathbf{q}$). The phase shifts originate from the complex amplitudes $\varphi_{\mathrm{f}} = \angle\hat{U}_{\mathrm{f}}$ and $\varphi_{\mathrm{s}} = \angle\hat{U}_{\mathrm{s}}$.

Inserting ansatz (16) into the reduced equation of motion (10)

$$\left[\delta^2\mathbf{M} + \delta\mathbf{D} + \mathbf{C}\right]\hat{\mathbf{q}} = \mathbf{0} \quad \text{with} \quad \hat{\mathbf{q}} = \begin{bmatrix} \hat{U}_{\mathrm{f}} \\ \hat{U}_{\mathrm{s}} \end{bmatrix} \qquad (18)$$

has only nontrivial $\hat{\mathbf{q}} \neq \mathbf{0}$ solutions, if the determinant vanishes

$$\det\left[\delta^2\mathbf{M} + \delta\mathbf{D} + \mathbf{C}\right] = 0. \qquad (19)$$

Evaluation of this determinant gives the characteristic equation

$$p_{\mathrm{char}}(\delta) = a_4\delta^4 + a_3\delta^3 + a_2\delta^2 + a_1\delta + a_0 = 0, \qquad (20)$$

with

$$a_4 = \frac{m_1 m_2}{m_1 + m_2} + m_\Delta, \qquad (21a)$$

$$a_3 = d_\Delta, \qquad (21b)$$

$$a_2 = \frac{m_1 + m_\Delta}{m_1 + m_2}c_2, \qquad (21c)$$

$$a_1 = \frac{c_2}{m_1 + m_2}d_\Delta, \qquad (21d)$$

$$a_0 = 0. \qquad (21e)$$

We immediately notice the eigenvalue $\delta_0 = 0$ as a trivial solution to the quartic equation (20). Substitution of $\delta_0 = 0$ into (18) yields the eigenmode $\mathbf{r} = [1, 0]^{\mathrm{T}}$ corresponding to m_1 in arbitrary position and m_2 in unstressed position, both at rest, which is plausible as there is no force from dashpot or mass coupling. From the remaining cubic equation, we know that it has either one real and two conjugate-complex roots, or three (individual or multiple) real roots[1]. However, we postpone

---

[1]This can be intuited by drawing a typical third-order polynomial and shifting it up and down along the ordinate.

the root-finding discussion to section 4, where we will encounter a quartic equation again, but with different coefficients. Indeed, the present characteristic equation (20) for the S-wave model is a special case ($a_0 = 0$) of the upcoming characteristic equation (37) for the P-wave model. For now, we anticipate that there is one real root (decay) and a pair of conjugate-complex roots (oscillation) for physically plausible parameters. Since the oscillation corresponds to waves, we conclude that S-waves always exist. With our exemplary values (appendix A) we notice an exponential decay in the first mode, in which both masses slow down while moving in opposite direction

$$\delta_1 = -334.543, \qquad (22a)$$

$$\mathbf{r}_1 = \begin{bmatrix} 0.970 \\ -0.244 \end{bmatrix}. \qquad (22b)$$

The second mode is composed of the pair of conjugate-complex roots

$$\delta_2 = \bar{\delta}_3 = -0.0011 - 1.8127\mathrm{i}, \qquad (23a)$$

$$\mathbf{r}_2 = \bar{\mathbf{r}}_3 = \begin{bmatrix} 0.7071 \\ 0.7071 - 0.0043\mathrm{i} \end{bmatrix}, \qquad (23b)$$

corresponding to a damped oscillation (real part of eigenvalues corresponds to decay constant and imaginary part to angular frequency), which is slightly phase shifted (complex-valued eigenvector) for the base mode ($k = 0$) in our example.

Having found the eigenvalues δ_i, finding the corresponding eigenvectors for a 2D system is easy: we may choose any of the two lines from the equation of motion (10). Here, we find from the first line (same result from the second) after evaluation of the ansatz (16)

$$\frac{\hat{U}_{\mathrm{f}i}}{\hat{U}_{\mathrm{s}i}} = \frac{m_\Delta\delta_i^2 + d_\Delta\delta_i}{(m_1 + m_\Delta)\delta_i^2 + d_\Delta\delta_i}. \qquad (24)$$

As customary, we constrain the eigenvectors to unit length $\sqrt{\hat{U}_{\mathrm{f}i}^2 + \hat{U}_{\mathrm{s}i}^2} = 1$.

So far we focused on the base mode ($k = 0$). Now, we sweep through higher modes ($k > 0$), and compute the characteristics of the reduced S-model (phase angle, amplitude) and its wave characteristics (velocity, decay). The amplitudes and phase shifts decoded in the eigenvalues- and vectors are illustrated in figure 3 for selected modes. We notice from the numerical results that the imaginary part of the complex eigenvalue and thus the frequency f increases with mode number k. Consequently, we evaluate the wave and oscillation characteristics for various frequencies, shown in figures 4 and 5. The results can be interpreted as follows:
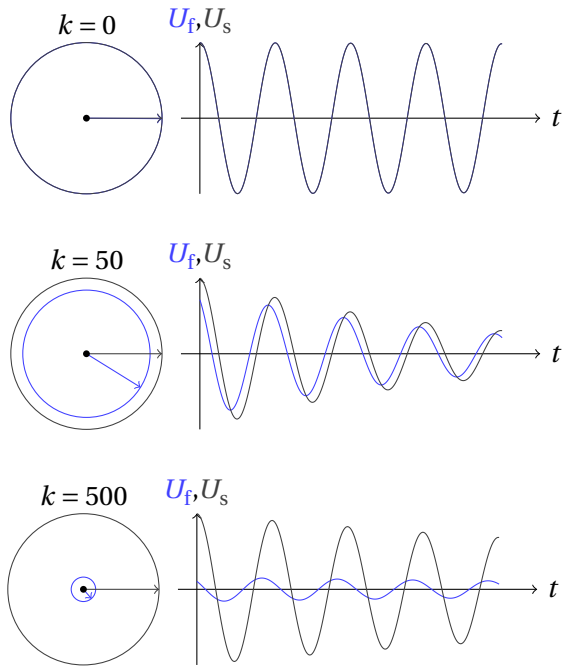
Figure 3 – Complex amplitudes and transient oscillation of S-wave model in base frequency (top) where both lines closely overlay, near the characteristic frequency f_c (middle) and beyond (bottom), with time axis being scaled to the period of the free oscillations.

- at low frequencies, the shear waves are slow because inertia is high and dissipation is low (fluid and solid move in phase),
- at intermediate frequencies a transition occurs accompanied by a dissipation peak (fluid and solid move out of phase at moderate amplitudes),
- at high frequencies the shear waves are fast because inertia is low (mainly solid moves),

Note that the edgy beginning of these curves is due to the discretization into modes (integer k).

The computation of the phase velocity $c = f\lambda$ (valid for either wave type) assumes a wavelength equal to a multiple of domain length (here $\lambda = 4$, since the assumed mode shape covers a quarter of the spatial period $\frac{\pi}{2} = \frac{1}{4}2\pi$), which is exact for undamped waves and an approximation for damped waves [8].

For comparison, in an elastic media with constant parameters the non-dimensional shear wave velocity were constant $c_S^{el} = 0.61$ over frequency for our example, and by definition the non-dimensional phase velocity of elastic P-waves were constant $c_P^{el} = 1$, too. Of course in elastic media, no dissipation would be observed.
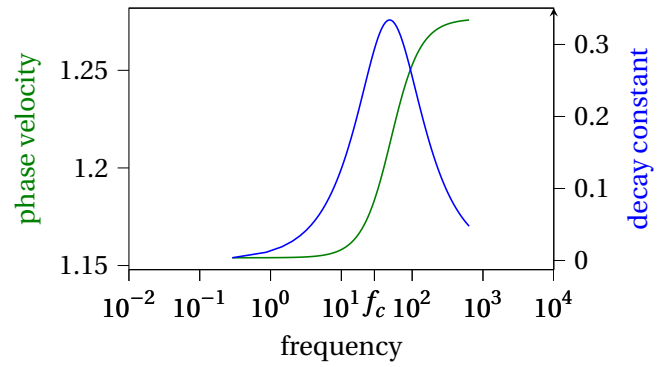
Figure 4 – Phase velocity (sigmoid curve up) and decay constant (bell curve) of S-waves versus frequency.
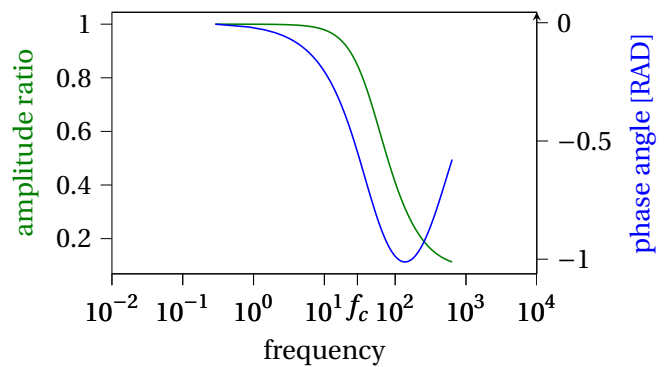
Figure 5 – Amplitude ratio fluid-to-solid (sigmoid curve down) and phase angle (bell curve down) of S-waves versus frequency.
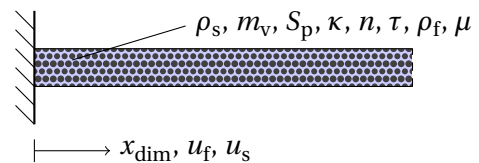
Figure 6 – Continuous model for P-waves: one-dimensional, poroelastic bar with fixed, undrained left end ($x_{dim} = 0$) and free, drained right end ($x_{dim} = L$).
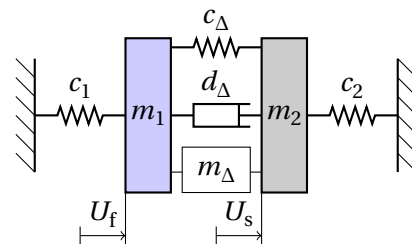
Figure 7 – Multibody-system representing a reduced model for P-waves in a poroelastic bar.

3 Model Reduction of P-Waves

We consider again a one-dimensional, poroelastic wave-guide on a finite domain as shown in figure 6. This time the displacements are in longitudinal direction in contrast to the transversal displacements in the previous section about S-waves. From the original PDEs [14, chapter 5.2] we obtained a non-dimensional formulation, as we did before in section 2. The motion is governed by the balance of momentum of the fluid phase (displacement u_f) and of the solid phase (displacement u_s)

$$\frac{n}{\rho}\ddot{u}_\mathrm{f} + \frac{n\tau}{\rho}\big(\ddot{u}_\mathrm{f} - \ddot{u}_\mathrm{s}\big) + nD_\mathrm{P}\big(\dot{u}_\mathrm{f} - \dot{u}_\mathrm{s}\big)$$
$$- nM\big(nu_\mathrm{f}'' - (n-\alpha)u_\mathrm{s}''\big) = 0, \quad (25a)$$

$$(1-n)\ddot{u}_\mathrm{s} - \frac{n\tau}{\rho}\big(\ddot{u}_\mathrm{f} - \ddot{u}_\mathrm{s}\big) - nD_\mathrm{P}\big(\dot{u}_\mathrm{f} - \dot{u}_\mathrm{s}\big)$$
$$- (n-\alpha)M\big(-nu_\mathrm{f}'' + (n-\alpha)u_\mathrm{s}''\big) - u_\mathrm{s}'' = 0, \quad (25b)$$

which is identical with the shear wave PDE (2), except the displacement coupling between solid and fluid (stiffness) and different dissipation ratio (D_P instead of D_S).

Further we assume fixed, undrained boundary conditions (no displacement, no fluid flow) on the left and free, drained boundary conditions (force free, fluid flows freely) on the right, which mathematically coincide with boundary conditions (5). Note that for non-degenerate parameters

$$0 < m_\mathrm{v}, S_\mathrm{p} < \infty,$$

the drained boundary condition implies $u_\mathrm{f}'(t,1) = 0$ and similarly the boundary condition of no normal stress implies $u_\mathrm{s}'(t,1) = 0$. The non-dimensional parameters

$$\rho = \frac{\varrho_\mathrm{s}}{\varrho_\mathrm{f}}, \qquad (26)$$

$$M = \frac{m_\mathrm{v}}{S_\mathrm{p}}, \qquad (27)$$

$$D_\mathrm{P} = \frac{n\mu L\sqrt{m_\mathrm{v}}}{\kappa\sqrt{\varrho_\mathrm{s}}} \qquad (28)$$

depend on the dimensional parameters fluid density ϱ_f, solid density ϱ_s, one-dimensional compressibility (i.e. inverse of P-wave modulus) of the bulk $m_\mathrm{v} = \left(K + \frac{4}{3}G\right)^{-1}$, storativity $S_\mathrm{p} = nC_\mathrm{f} + (\alpha - n)C_\mathrm{s}$, fluid viscosity μ, permeability κ as well as on the originally non-dimensional parameters porosity n ($0 < n < 1$), Biot coefficient α ($n < \alpha \leq 1$) and tortuosity factor τ as defined by Verruijt [14]. They are non-negative real ($\rho, M, D_\mathrm{P}, \alpha, n, \tau \in \mathbb{R}_0^+$) on physical grounds. In comparison to S-waves we have

the same parameter ρ, a new parameter M and the following relation

$$D_\mathrm{S} = \frac{c_\mathrm{P}^\mathrm{el}}{c_\mathrm{S}^\mathrm{el}} D_\mathrm{P} \quad \text{with} \quad \frac{c_\mathrm{P}^\mathrm{el}}{c_\mathrm{S}^\mathrm{el}} = \sqrt{\frac{1}{m_\mathrm{v}G}}. \qquad (29)$$

We note that Biot [1] refers to the phase velocity of undrained waves

$$c_\mathrm{P}^\mathrm{un} = \sqrt{\frac{1/m_\mathrm{v} + \alpha^2/S_\mathrm{p}}{(1-n)\varrho_\mathrm{s} + n\varrho_\mathrm{f}}}, \qquad (30)$$

which means the fluid cannot flow out, thus it stiffens the bulk (remember m_v denotes bulk compressibility, i.e., of the porous matrix which is softer than the pure solid). Whereas we use the phase velocity in the elastic solid

$$c_\mathrm{P}^\mathrm{el} = \frac{1}{\sqrt{m_\mathrm{v}\varrho_s}}, \qquad (31)$$

which is usually smaller than the undrained velocity ($c_\mathrm{P}^\mathrm{el} < c_\mathrm{P}^\mathrm{un}$), for non-dimensionalization, because the resulting relations are simpler. We will discuss this difference in section 5.

Again we make use of a Galerkin-ansatz; indeed, we use the same functions (6) as in section 2. The resulting reduced equation of motion coincides with equation (10). Although its coefficients differ, the matrices $\mathbf{M}$ and $\mathbf{D}$ share the same structure with their counterparts of the S-wave model. However, the stiffness matrix is different in structure

$$\mathbf{C} = \begin{bmatrix} c_1 + c_\Delta & -c_\Delta \\ \text{sym.} & c_2 + c_\Delta \end{bmatrix}, \qquad (32)$$

which is reflected in the corresponding discrete system shown in figure 7. Except the mass coupling m_Δ, all parameters have a common interpretation for multibody-systems as masses, dashpots or springs. Again, evaluation of the swap relation (15) confirms that the damping is non-modal, except for degenerate parameter values.

Note that for constant parameters, there is no other dependency on x than the ansatz and weight function. In fact, we have the same Galerkin integrals (9) as before. The matrix entries are related with the non-dimensional,

continuum parameters as follows

$$m_1 = I_{11}\frac{n}{\rho}, \tag{33a}$$

$$m_2 = I_{22}(1-n), \tag{33b}$$

$$m_\Delta = I_{12}\frac{n\tau}{\rho}, \tag{33c}$$

$$d_\Delta = I_{12}nD_P, \tag{33d}$$

$$c_1 = I_{11}\left(\frac{\pi}{2}\right)^2 nM\alpha, \tag{33e}$$

$$c_2 = I_{22}\left(\frac{\pi}{2}\right)^2\left(1-(n-\alpha)M\alpha\right), \tag{33f}$$

$$c_\Delta = I_{12}\left(\frac{\pi}{2}\right)^2 nM(n-\alpha). \tag{33g}$$

Further inspection reveals that all parameters are real and except c_Δ all of them are non-negative (m_1, m_2, m_Δ, d_Δ, c_1, $c_2 \in \mathbb{R}^+$ and $c_\Delta \in \mathbb{R}$). The system remains stable, as long as stiffness matrix and mass matrix are positive definite $\mathbf{C}, \mathbf{M} > 0$, which by the structure of these matrices reduces to the conditions

$$c_\Delta > -\frac{c_1 c_2}{c_1 + c_2}, \tag{34a}$$

$$m_\Delta > -\frac{m_1 m_2}{m_1 + m_2}. \tag{34b}$$

These conditions are met for physically plausible systems with $\alpha > n > 0$, as found from insertion of (33g), (33e) and (33f) into (34a) remembering (9)

$$nM(n-\alpha) > -\frac{nM\alpha\left(1-(n-\alpha)M\alpha\right)}{nM\alpha + 1 - (n-\alpha)M\alpha} \tag{35}$$

and simplification to

$$n^2 M > 0, \tag{36}$$

what we already assumed on physical grounds. It goes without saying that condition (34b) is met, since the masses are non-negative $m_1, m_2, m_\Delta \geq 0$.

4 Modal Analysis

Now we are going to solve the free vibration problem of the reduced model for P-waves, i.e., equation (10) with parameters (33). We again use the exponential ansatz (16), which on insertion into the reduced equation of motion (10) and requesting linear dependence leads to the characteristic equation

$$p_{\text{char}}(\delta) = a_4\delta^4 + a_3\delta^3 + a_2\delta^2 + a_1\delta + a_0 = 0. \tag{37}$$
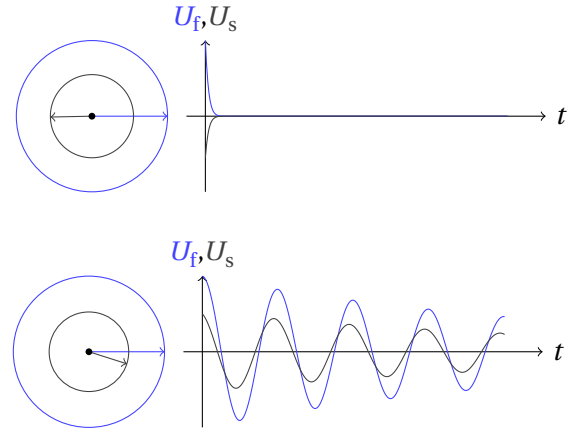
Figure 8 – Complex amplitudes and transient oscillation of slow P-wave (top) and fast P-wave (bottom) in first mode where slow P-wave occurs ($k = 5$).

For the current model, the coefficients read

$$a_4 = \frac{m_1 m_2}{m_1 + m_2} + m_\Delta, \tag{38a}$$

$$a_3 = d_\Delta, \tag{38b}$$

$$a_2 = \frac{m_2 + m_\Delta}{m_1 + m_2}c_1 + \frac{m_1 + m_\Delta}{m_1 + m_2}c_2 + c_\Delta, \tag{38c}$$

$$a_1 = \frac{c_1 + c_2}{m_1 + m_2}d_\Delta, \tag{38d}$$

$$a_0 = \frac{c_1 c_2 + c_\Delta(c_1 + c_2)}{m_1 + m_2}. \tag{38e}$$

The characteristic equation of the P-wave model (38) reduces to the characteristic equation of the S-wave model (21) for $c_1 = c_\Delta = 0$. In other words, although the parameters, e.g., mass m_1, have different values in both models (S- and P-wave) there is a common mathematical structure. On closer inspection, we find that all coefficients are non-negative $a_i \geq 0$, which is straightforward except for $i = 2$. For a_2, we find the limit case from condition (34) leading to

$$a_2 \geq \frac{(c_1 m_2 - c_2 m_1)^2}{(c_1 + c_2)(m_1 + m_2)^2} \geq 0. \tag{39}$$

The characteristic equation (37) is a quartic equation and its discriminant D_4, given by equation (41) in appendix B, helps us to determine the transition from asymptotic decay to oscillation, i.e., the threshold from which on slow P-waves exist. Generally, for real coefficients $a_0, a_1, a_2, a_3, a_4 \in \mathbb{R}$ we know [11]:

$D_4 < 0$ two real roots and

            one conjugate-complex pair,

$D_4 = 0$ at least two roots are equal,

$D_4 > 0$ four real roots or

            two conjugate-complex pairs.
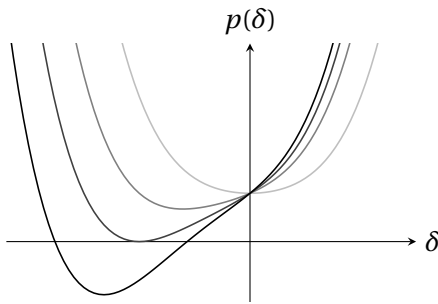
Figure 9 – Quartic polynomial with positive coefficients, opacity of lines corresponds to asymmetry introduced by cubic and linear monomials, here exemplary for $p(\delta) = a_4\delta^4 + a_3\delta^3 + a_2\delta^2 + a_1\delta + a_0$ with $a_4 = a_2 = a_0 = 1$ and $a_3 = a_1 = 0\ldots1.9$.

Furthermore, from the coefficients (38) we find that d_Δ is decisive, as it introduces asymmetry ($d_\Delta > 0$) and without dissipation ($d_\Delta = 0$) the polynomial $p(\delta)$ would be symmetric to the y-axis.

Similarly to equation (24) of the S-wave model we find the eigenvectors of the P-wave model. The free oscillations corresponding to the two modes are shown in figure 8 illustrating that the mode corresponding to the slow P-wave decays much faster. This faster decay of slow P-waves will be attributed to the phase shift and amplitude ratio in the next section.

5 Discussion

We have identified four eigenvalues δ_i ($i = 1,2,3,4$) with corresponding eigenvectors and now need to determine whether they lead to damped oscillations or aperiodic decay. Two real roots lead to real coefficients, i.e., aperiodic motion (here slow and fast decay), whereas a pair, i.e., two roots, which are conjugate-complex roots, lead to damped oscillations. A combination of two eigenvalues/-vectors is necessary to match initial positions $u_f(0, x)$ and $u_s(0, x)$, as well as initial velocities $\dot{u}_f(0, x)$ and $\dot{u}_s(0, x)$. By the signs $a_i \in \mathbb{R}_0^+$ of coefficients (38), there are only two possible cases, which are shown in figure 9. Either two complex conjugated pairs (corresponds to two damped oscillations), or two real roots and one complex conjugated pair (corresponds to two decays and one damped oscillation). In the special case (20) for S-waves, the graph passes the origin and only two cases remain: the symmetric case ($d_\Delta = 0$) with a multiple real root in the origin, and the asymmetric case ($d_\Delta > 0$) with two real roots, one at the origin $\delta = 0$ and another negative one $\delta < 0$.

This motivates a closer look at the discriminant D_4 in dependence on d_Δ which is shown in figure 10, where
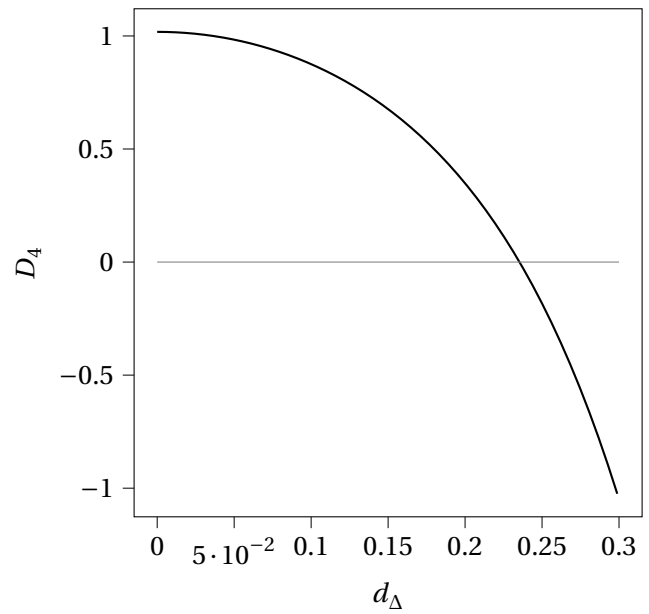
Figure 10 – For damping below a critical value ($d_\Delta < d_{\Delta\mathrm{crit}}$) there are two damped oscillations ($D_4 > 0$), otherwise exponential decay, slow and fast, and one damped oscillation ($D_4 < 0$).

we observe one zero crossing. In our example there exists no slow P-wave in the base mode ($k = 0$), since there the dissipation is above the critical value

$$d_\Delta = 13.900 > d_{\Delta\mathrm{crit}} = 0.235. \tag{40}$$

To obtain the characteristics of slow and fast P-waves we sweep through higher modes ($k > 0$). Slow P-waves start to exist from a certain threshold on and then increase monotonically in phase velocity and decrease monotonically in decay constant with increasing frequency, as shown in figure 11 and explainable by the amplitude ratio and phase shift from figure 12. Fast P-waves increase in phase velocity with increasing frequency and a peak in the decay constant around Biot's characteristic frequency, as shown in figure 13 and explainable by figure 14, which is qualitatively similarly to S-waves. A phase velocity of $c_P = 1$ means as fast as the elastic P-wave due to our choice for non-dimensionalization. For information, the non-dimensional phase velocity of undrained waves in our example is $c_P^{\mathrm{un}} = 3.827$.

What remains is to relate our non-dimensionalization with Biot's reference values, i.e., we come back to different definitions of the reference velocity mentioned in the beginning. Biot, as apparent from equations (5.4) and (7.4) in his paper [1], refers to the velocity (30) of P-waves in the undrained case, he uses the symbol V_c, and a characteristic frequency, given by equation (1), which separates the low- from the high-frequency range. In our example its non-dimensional value is $f_c = 29.312$.
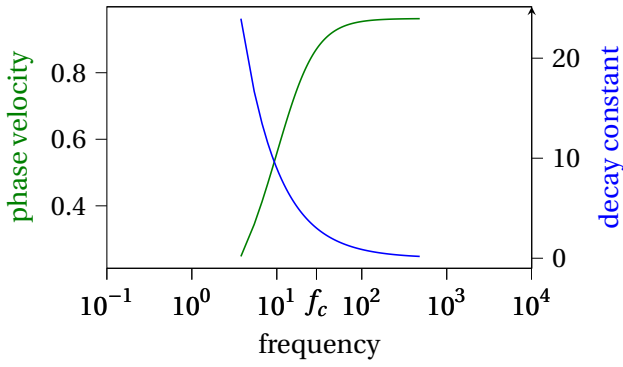
Figure 11 – Phase velocity (asymptotic curve up) and decay constant (asymptotic curve down) of slow P-waves versus frequency.

Finally, we would like to give some interpretation of the multibody-system parameters of the oscillator shown in figure 7, particularly the interaction of the fluid with the solid (relative motion between m_1 representing fluid and m_2 representing solid) shown in figure 15. From the structure of the matrices we may recognize that the parameters with index $\square_\Delta$ refer to key solid-fluid interaction phenomena in porous media:

- m_Δ undirected acceleration / inertia due to redirection of flow along tortuous paths (viz. tortuosity τ), cf. figure 15.
- d_Δ solid-fluid momentum exchange due to frictional interaction between solid and fluid (viz. viscosity μ and permeability κ).
- c_Δ expresses the differences in stiffness between fluid and solid. When the fluid is incompressible, it has to be squeezed out of the solid matrix due to volumetric strain imparted by P-waves (not existent in S-waves). On the other hand, when it is compressible, the fluid can be compressed in the pore space upon passage of the P-wave, reducing the amount of flow necessary to comply with mass balance considerations.

For further study we suggest to take a closer look at the parameter dependencies and their effect on the frequency characteristics, particularly of slow P-waves. For this purpose the Jupyter Notebook accompanying this article can serve as a valuable study aid in the sense of experimental numerics [7].

6 Summary and Outlook

Oscillations are easier to describe than waves and still capture crucial consequences of Biot's theory. With this approach, one perceives the slow P-wave as a motion of the pore fluid relative to the solid with larger amplitude
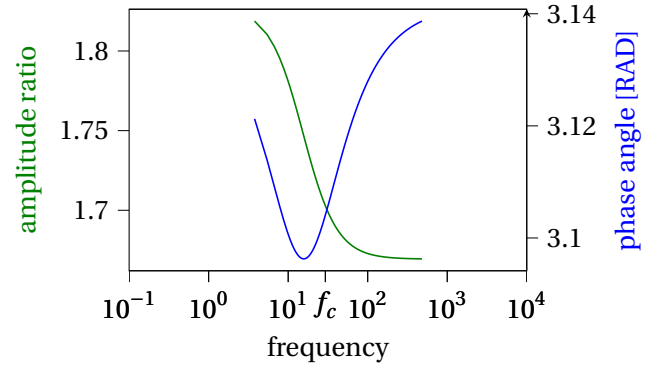
Figure 12 – Amplitude ratio fluid-to-solid (sigmoid curve down) and phase angle (bell curve down) of slow P-waves versus frequency, the edgy beginning of the curves is due to the discretization into modes (integer k).
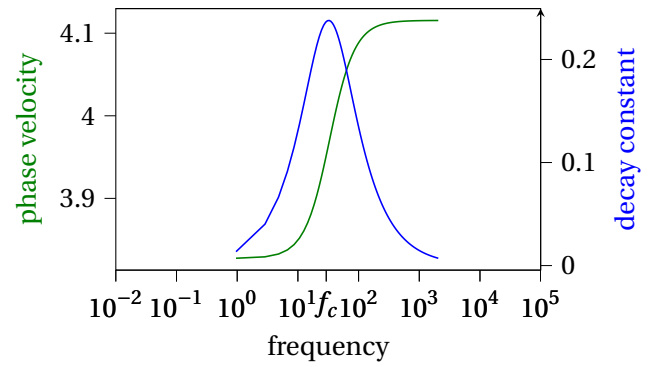
Figure 13 – Phase velocity (sigmoid curve up) and decay constant (bell curve) of fast P-waves versus frequency.
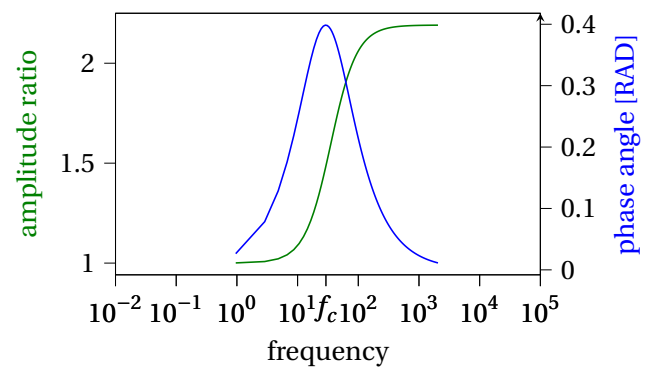
Figure 14 – Amplitude ratio fluid-to-solid (sigmoid curve up) and phase angle (bell curve) of fast P-waves versus frequency, the edgy beginning of the curves is due to the discretization into modes (integer k).
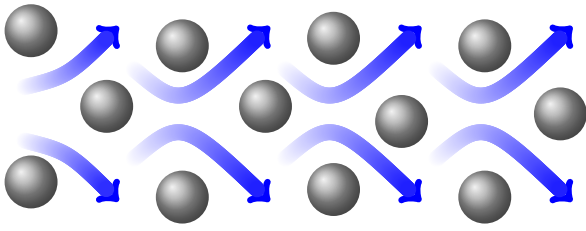
Figure 15 – Fluid flow between solid grains.

ratios and phase shifts than fast P-waves and thus being much more dissipative.

We hope the simplified model of a two degree-of-freedom oscillator is a helpful tool for understanding waves in poroelastic media. Nevertheless, even this simple model raises further questions, the reader might find worthy of investigation, that are beyond the scope of this paper, e.g.: how does the illustrated behavior depend on the poroelastic parameters, what is the meaning of forced oscillations and its effects such as resonance and absorption?

Code Availability: The code behind the simulations is provided as a Jupyter notebook. It can be found on GitHub[2] or spun up on MyBinder[3]. The source code is available as supplementary material and can be obtained under

DOI:10.14464/gammas.v6i1.663

A   Numerical Values

As numerical values, except for tortuosity τ and one-dimensional bulk compressibility m_v, we use Verruijt's example, from chapter 5.4.4. of his textbook [14], for our plots. Our numerical values are listed in Tables 1, 2, 3 and 4. Note, that the multibody-system (MBS) parameters are non-dimensional, since they are derived from a non-dimensional formulation.

---

[2] https://github.com/nagelt/soil_dynamics/blob/master/extra_biot_oscillations.ipynb

[3] https://mybinder.org/v2/gh/nagelt/soil_dynamics/HEAD?labpath=extra_biot_oscillations.ipynb

Table 1 – Dimensional parameters

length	L	$20\,\mathrm{m}$
solid density	ϱ_s	$2650\,\mathrm{kg\,m^{-3}}$
fluid density	ϱ_f	$1000\,\mathrm{kg\,m^{-3}}$
permeability	κ	$1 \times 10^{-10}\,\mathrm{m^2}$
fluid viscosity	μ	$1 \times 10^{-3}\,\mathrm{Pa\,s}$
bulk compressibility	m_v	$2 \times 10^{-9}\,\mathrm{Pa^{-1}}$
storativity	S_p	$2 \times 10^{-10}\,\mathrm{Pa^{-1}}$

Table 2 – Non-dimensional parameters

bulk Poisson's ratio	ν	0.2
Biot coefficient	α	1.0
porosity	n	0.4
tortuosity	τ	0.1
density ratio	ρ	2.65
stiffness ratio	M	10.00
dissipation ratio (S-wave)	D_S	113.49
dissipation ratio (P-wave)	D_P	69.50

Table 3 – MBS parameters of the S-wave model

fluid mass	m_1	0.0755
solid mass	m_2	0.3000
mass coupling (fsi)	m_Δ	0.0075
damping (fsi)	d_Δ	22.6985
solid stiffness	c_2	1.2337

Table 4 – MBS parameters of the P-wave model

fluid mass	m_1	0.0754
solid mass	m_2	0.3000
mass coupling (fsi)	m_Δ	0.0075
damping (fsi)	d_Δ	13.9000
fluid (channel) stiffness	c_1	4.9348
solid stiffness	c_2	8.6359
stiffness (fsi)	c_Δ	−2.9609

B Discriminant of Quartic Polynomials

The ready-to-use formula is given by Schroeppel[4]

$$
\begin{aligned}
D_4 = &\; 256a_4^3 a_0^3 - 192a_4^2 a_3 a_1 a_0^2 - 128a_4^2 a_2^2 a_0^2 \\
&+ 144a_4^2 a_2 a_1^2 a_0 - 27a_4^2 a_1^4 + 144a_4 a_3^2 a_2 a_0^2 \\
&- 6a_4 a_3^2 a_1^2 a_0 - 80a_4 a_3 a_2^2 a_1 a_0 + 18a_4 a_3 a_2 a_1^3 \\
&+ 16a_4 a_2^4 a_0 - 4a_4 a_2^3 a_1^2 - 27a_3^4 a_0^2 + 18a_3^3 a_2 a_1 a_0 \\
&- 4a_3^3 a_1^3 - 4a_3^2 a_2^3 a_0 + a_3^2 a_2^2 a_1^2. \quad (41)
\end{aligned}
$$

Actually that is enough for us, but there are further *sub-discriminants* to narrow down the root distribution. There are things to learn here, too, such as the representation as a determinant of the Sylvester matrix with coefficients of the polynomial and of its derivative[5], and the relation with their greatest common divisor, e.g., computed by (extended) Euklid's algorithm (algebra meets analysis!). Since discrimination of roots is not the main purpose of the paper, we encourage interested readers to explore this interesting topic in greater depth on their own initiative [11].

References

[1] Maurice A. Biot. Theory of propagation of elastic waves in a fluid-saturated porous solid – I. low frequency range. *The Journal of the Acoustical Society of America*, 28(2):164–178, 1956. doi: 10.1121/1.1908239.

[2] Maurice A. Biot. Theory of propagation of elastic waves in a fluid-saturated porous solid – II. higher frequency range. *The Journal of the Acoustical Society of America*, 28(2):179–191, 1956. doi: 10.1121/1.1908241.

[3] Marc S. Boxberg, Jean H. Prévost, and Jeroen Tromp. Wave Propagation in Porous Media Saturated with Two Fluids. *Transport in Porous Media*, 107(1):49–63, mar 2015. ISSN 0169-3913. doi: 10.1007/s11242-014-0424-2.

[4] Alexander H.-D. Cheng. *Poroelasticity*, volume 27. Springer International Publishing, 2016. ISBN 978-3-319-25200-1. doi: 10.1007/978-3-319-25202-5.

[5] Peter Hagedorn and Anirvan DasGupta. *Vibrations and waves in continuous mechanical systems*. John Wiley & Sons, 2007. ISBN 9780470518427.

[6] Peter Hagedorn and Daniel Hochlenert. *Technische Schwingungslehre: Schwingungen linearer diskreter mechanischer Systeme*. Deutsch, 2012. ISBN 9783808556962.

[7] Dominik Kern and Thomas Nagel. An experimental numerics approach to the terrestrial brachistochrone. *GAMM Archive for Students*, 4(1), Jul. 2022. doi: 10.14464/gammas.v4i1.512.

[8] Anja Kühne. Damping-induced dispersion in simple waveguides. *GAMM Archive for Students*, 5(1), May 2023. doi: 10.14464/gammas.v5i1.587.

[9] Hans P. Langtangen and Geir K. Pedersen. *Scaling of Differential Equations*. Simula SpringerBriefs on Computing. Springer International Publishing, 2016. ISBN 9783319327266.

[10] Gjerrit Meinsma. Dimensional and scaling analysis. *SIAM Review*, 61(1):159–184, 2019. doi: 10.1137/16M1107127.

[11] Nikola Obreshkov. *Verteilung und Berechnung der Nullstellen reeller Polynome*. Hochschulbücher für Mathematik. VEB Deutscher Verlag der Wissenschaften, 1963. ISBN 9789544309374.

[12] Thomas J. Plona. Observation of a second bulk compressional wave in a porous medium at ultrasonic frequencies. *Applied Physics Letters*, 36(4):259–261, 1980. doi: 10.1063/1.91445.

[13] Holger Steeb, Patrick S. Kurzeja, and Stefan M. Schmalholz. Wave propagation in unsaturated porous media. *Acta Mechanica*, 225(8):2435–2448, aug 2014. ISSN 0001-5970. doi: 10.1007/s00707-014-1135-z.

[14] Arnold Verruijt. *An Introduction to Soil Dynamics*. Springer Netherlands, 2010. ISBN 978-90-481-3440-3.

[15] Arnold Verruijt. *An Introduction to Soil Mechanics*. Theory and Applications of Transport in Porous Media. Springer International Publishing, 2017. ISBN 9783319611853.

---

[4]www.inwap.com/pdp10/hbaker/hakmem/geometry.html

[5]demonstrations.wolfram.com/DiscriminantOfAPolynomial